



15th Canadian Masonry Symposium
Ottawa, Canada
June 2-5, 2025



Experimental Study of Reinforced Masonry Columns

Yi Liuⁱ

ABSTRACT

This paper presents the results of an experimental study on masonry columns subjected to concentric and eccentric axial loads until failure. A review of available literature revealed limited experimental studies and data on masonry columns over the past four decades. The current Canadian masonry design standard applies the same provisions for masonry columns as for masonry walls. This study aimed to investigate the behaviour and strength of reinforced masonry columns, providing new physical data using current masonry products and building techniques. Additionally, the results were used to verify the efficacy of design provisions for masonry columns in both the Canadian and American masonry design standards, with a focus on the moment magnifier method.

Six masonry columns with slenderness ratios (kh/t) ranging from 6.3 to 15.8 were tested. For each slenderness ratio, two cross-section configurations—constructed with either stretcher blocks or C-shaped blocks—were studied. The experimental results revealed that the failure modes of the specimens depended on their slenderness and loading conditions. At low slenderness and under concentric axial load, failure was characterized by splitting longitudinal cracks and localized crushing, leading to the buckling of longitudinal reinforcement. At higher slenderness and under eccentric axial load, failure was characterized by flexural tensile cracking and compressive crushing, primarily around the midspan of the specimens. As slenderness increased, the capacity of the specimens decreased, with pronounced nonlinearity at the outset of loading.

The comparison with design values highlighted the design difference in Canadian and American design provisions. The possible causes for this difference were discussed in the paper.

KEYWORDS

Masonry columns, slenderness effect, eccentric compression loading, moment magnifier method, experimental study

ⁱ Professor, Dalhousie University, Halifax, Canada, Yi.liu@dal.ca



INTRODUCTION

In modern masonry construction, masonry columns are frequently used as compressive members either as a stand-alone element or integrated into a masonry wall. Masonry materials, such as clay bricks and concrete masonry blocks, are the material of choice for construction of masonry columns. While both materials are common, this study focuses on concrete masonry blocks due to their prevalent use in North America for structural application. Masonry columns are typically defined as vertical compression members with a height exceeding five times their thickness and a length less than three times their thickness [1]. Although reinforced masonry (RM) columns share similarities to reinforced concrete (RC) columns, the difference between the modular nature of the former and the monolithic nature of the latter makes them essentially different structural elements with their own behavioural characteristics.

While significant research has been conducted on RC columns, studies on RM columns have been limited. Early work by Sturgeon et al. [2] and Edgell & Templeton [3] highlighted the effect of reinforcement and slenderness on the behaviour of masonry columns. Common failure modes include splitting and crushing for unreinforced columns, while reinforced columns experience face-shell spalling and reinforcement buckling. As modern construction usually incorporate reinforcement, the slenderness effect becomes the focus of RM column studies. A general approach for considering the slenderness effect of RM columns has been through the moment magnifier method with a modified Euler buckling load. A key parameter in the modified Euler buckling load expression is the effective flexural rigidity, EI_{eff} , used to consider cracking of masonry and yielding of steel reinforcement at the buckling load. Much research has been concentrated on developing an accurate EI_{eff} expression to represent various material and geometric properties of RM compression members. A literature survey indicated that the existing studies in that respect has been mainly with RM walls ([4], [5], [6], [7]) and with little physical data on RM column tests. The methodology used for RM columns has thus been largely relied on that developed for RM walls where more test data is available.

Current design standards, such as the Canadian CSA S304-24 [1] and American TMS 402/602-16 [8], employ the moment magnifier method with the effective flexural rigidity to account for slenderness effects. However, the CSA S304 EI_{eff} equation is directly adopted from that developed for RM walls with limited experimental validation for columns. Studies by Liu [9] and Isfeld et al. [10] suggest this equation underestimates rigidity for walls, raising questions about its accuracy for columns. Further, TMS uses the same moment magnifier method but with a different EI_{eff} equation. This discrepancy between Canadian and American standards may lead to differing designs for identical material properties and loading conditions, underscoring the need for more experimental validation.

This study was then motivated to investigate the behaviour and capacity of RM columns, with a focus on flexural rigidity and its role in the moment magnifier method. Six RM columns with different design parameters were tested under both concentric and eccentric axial compression. In the latter case, single curvature bending was induced to magnify the secondary moment. The test results were used to examine the efficacy of both CSA and TMS design equations. Experimental observations and code comparisons are presented and discussed in the paper.

TEST SPECIMENS

A total of six RM column specimens was tested in the program. **Error! Reference source not found.** summarizes the specimens and their specific design parameters. These design parameters included effective slenderness ratio, kh/t , axial load eccentricity, e/t , and end eccentricity ratio, e_1/e_2 . The six specimens were divided into three groups based on their height, resulting in three slenderness ratios: short (S), intermediate (M), and tall (T). It is noted that a height of 3 meters is the maximum height that can be accommodated in

the laboratory and thus, the slenderness of 15.8 represents the limit achieved with the laboratory conditions and a label of “T” was used here for these specimens. Within each group, two column cross-section configurations were studied with approximately same dimensions, as depicted in Figure 1. Specimens made of stretcher blocks are labeled with “S” and those made of C-shape blocks are labeled with “C”. For example, specimen SS indicates a specimen with a short slenderness and constructed with stretcher blocks.

All masonry blocks were custom-made to the shown dimensions. For the stretcher block columns, two blocks were laid side-by-side and the orientation of two blocks were alternated for each course. For the C-shaped block columns, two C-shaped blocks were laid against each other to form a central cavity for grouting. For each specimen, #10M steel rebar was used as longitudinal reinforcement at each corner of the column and 3.65 mm steel wire was used as confinement ties at every other bed joint. The cover for longitudinal reinforcement was maintained at 50 mm for both cross-sections.

Table 1: RM Column Specimens

Number	Spec. ID	Height (mm)	Effective Slenderness Ratio (kh/t)	Cross Section Configuration	Axial Load Eccentricity (e/t)	Eccentricity Ratio (e_1/e_2)
1	SC	1200	6.3	C-Shaped Blocks	0	0
2	SS	1200	6.3	Stretcher Blocks	0	0
3	MC	2400	12.6	C-Shaped Blocks	1/3	+1
4	MS	2400	12.6	Stretcher Blocks	1/3	-1
5	TC	3000	15.8	C-Shaped Blocks	1/3	+1
6	TS	3000	15.8	Stretcher Blocks	1/3	+1

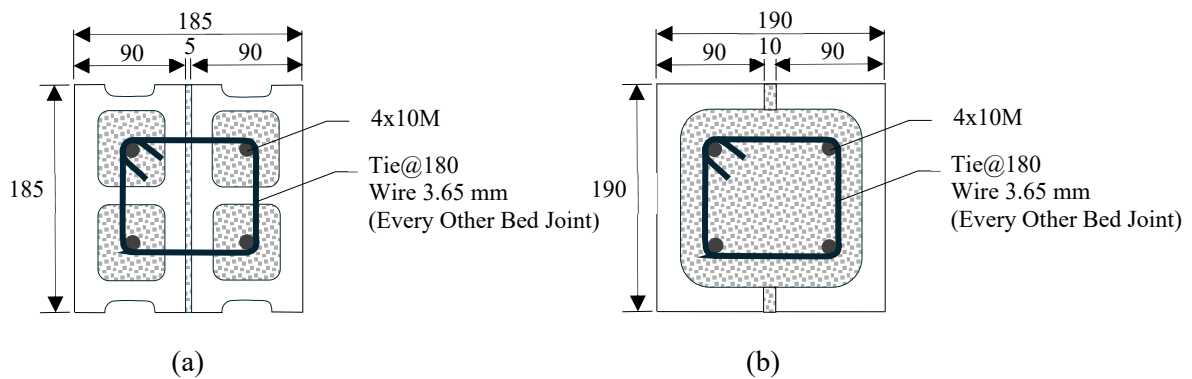


Figure 1: Cross-Section Configurations. (a) Stretcher Blocks; (b) C-Shaped Blocks

The specimens were constructed by a certified mason in a controlled laboratory environment. These specimens were constructed and cured in an upright position. For all specimens, the initial bed joint was placed first, and the blocks for each course were laid thereafter. The vertical reinforcement was introduced using a template at the bottom of the column to position the rebar accurately. Type S mortar was used and laid on all surfaces of the block. Pre-bent column ties were secured around the longitudinal reinforcements at the joint level of every other course. After laying the courses to the specimen’s desired final height,

grouting was conducted using high slump grout as per CSA A179 [11]. Once the construction of all columns was completed, they were cured for 28 days before testing commenced.

EXPERIMENTAL SETUP

All specimens were tested in a horizontal position using a 2 Mega Newton actuator. Figure 0 shows a schematic plan view of the entire testing assembly. Two concrete blocks, anchored to the strong floor using steel rods, served as reaction points for the specimen when the load was applied. The ends of the specimens were housed in a built-up plate assembly forming a “shoe”. Grout bags were used between the columns' ends and the steel plate assembly to ensure a uniform distribution of the load across the column cross-section, thereby preventing premature local crushing. The load was applied via a solid steel circular bar to the steel plate assembly at the specimen ends. Load eccentricity was achieved by positioning the steel bar to a pre-notched plate with the desired eccentricity. To offset the columns' self-weight when tested in a horizontal position, steel seat assemblies were positioned underneath the specimen at 1/3 of length intervals (not shown).

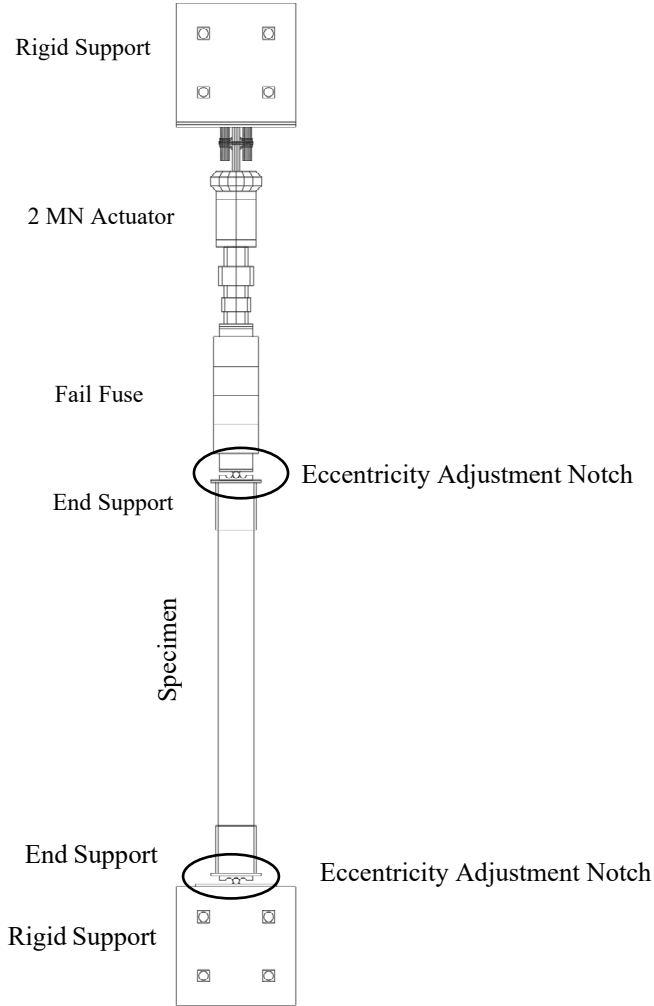


Figure 0: Schematic Plan View of the Test Setup

An electronic data acquisition system was used to record load, strain, and deformation data throughout the loading history. Lateral deformation was recorded at various points along the lengths of the columns using linear potentiometers (LP). Specimens also were instrumented with strain gauges on four longitudinal rebars at critical points of the columns to measure strains during testing. Before each test, the ends of the specimens were prepared where the extra length of the rebars was first cut off, and surfaces were ground to level. Each specimen was carefully transported to the testing position. Grout bags were then placed between the ends of each specimen and the loading plate assembly. The load cell, strain gauges, and LPs were inspected to ensure they functioned properly and were zeroed at the commencement of the test. The loading rate was set at 0.4 mm/min until failure. During each test, the cracking pattern, ultimate load, and failure mode were continuously observed and documented.

RESULTS AND DISCUSSION

Table provides a summary of the test results for column specimens, along with the masonry and steel rebar properties for each specimen obtained from auxiliary tests. It is noted that specimens constructed with stretcher blocks exhibited significantly lower masonry strength compared to those constructed with C-shaped blocks. Although the mortar and grout mix were used consistently for both constructions, the higher strength of the C-shaped block compared to the stretcher blocks, led to this pronounced difference in masonry strength.

Table 2: Test Results of the RM Specimens

Spec. ID	Effective Slenderness Ratio (kh/t)	Masonry		Steel		P _{cr} (kN)	P _{ult} (kN)
		f'_m (MPa)	E _m (MPa)	F _y (MPa)	F _t (MPa)		
SC	6.3	18.5	15,856			583	675
SS	6.3	8.5	7,482			392	468
MC	12.6	20.5	17,061			149	244
MS	12.6	7.9	7,896	381	571	-	95
TC	15.8	19.3	15,547			141	212
TS	15.8	9.5	9,307			97	147

Group “S” Specimens: SS and SC

These two specimens were 1200 mm high and tested under concentric compression. They were used as control specimens to obtain the compressive capacity of columns when the slenderness is not a concern. Figure 0 compares the axial load vs. axial deformation curves of specimens SS and SC. It can be seen that the C-shaped block specimen SC, had a higher capacity at both cracking and ultimate load when compared to the stretcher block specimen SS. This difference in capacity is expected as the masonry compressive strength f'_m for these two specimens was significantly different (8.5 vs 18.5 MPa). Both specimens began to show noticeable cracking around 85% of the ultimate load, and the load vs. axial deformation curves remained almost linear up to the cracking load, albeit that specimen SS showed a much lower stiffness. The failure occurred with significant spalling of masonry faceshell and buckling of axial reinforcement for both specimens.

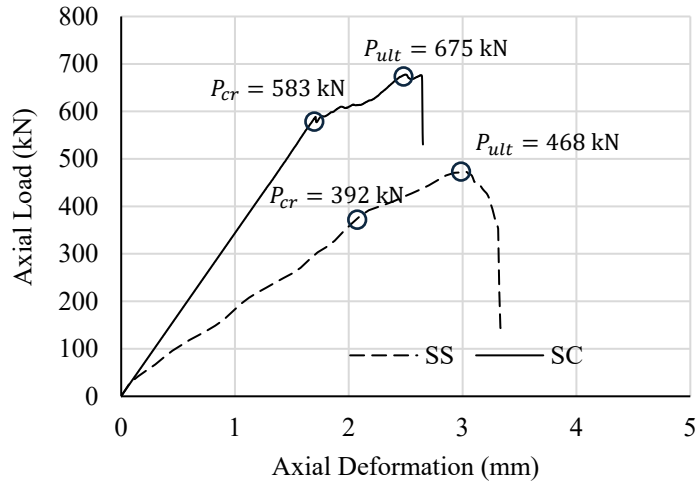


Figure 0: Axial Load vs Axial Deformation Curves of Group “S” Specimens

Group “M” Specimens: MS and MC

These two specimens had a height of 2400 mm and tested with a load eccentricity of $1/3t$ in a single curvature for MC and a reverse curvature for MS. Figure shows the load vs. midspan lateral deformation curve of specimen MC. The onset of nonlinearity began almost immediately after the application of load, which is attributed to the additional deformation due to the secondary moment, a typical behaviour for beam-columns. At approximately $P = 93$ kN, flexural cracks began to appear at midspan on the tension side of the column. As the tensile crack extended through the midspan mortar joint, crushing began to occur on the compression side around the midspan. The crushing caused spalling of the face shell and splitting of grouted cores on the compression side. The specimen failed at a load of $P_{ult} = 244$ kN when the longitudinal compressive reinforcement buckled on the compression side of the specimen. The failure mode is shown in (a) and (b).

Figure .

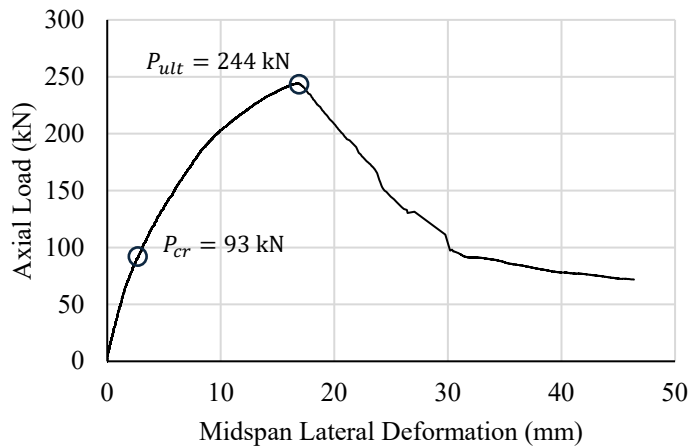


Figure 4: Load vs Midspan Lateral Deformation Curve for Specimen MC



(a)



(b)

Figure 5: Failure Mode of Specimen MC; (a) Plan View, (b) Close-Up View at Midspan

The test of Specimen MS was not successful as the specimen failed prematurely at the early stage of loading. It was discovered that the specimen was defective as its six bottom courses were not filled with grout despite effort was made during construction to fill the cores. This created a weak section where grout was not continuous, and the steel reinforcement was not continuously bonded to grout. The specimen failed suddenly at $P = 95$ kN at this location while the remainder of the specimen appeared to be intact. No reverse curvature behaviour was observed.

Group “T” Specimens: TS and TC

These two specimens had a height of 3000 mm and were tested under eccentric axial loads with an eccentricity of $1/3t$ in single curvature bending. Figure shows the axial load vs. midspan lateral deformation curves for both specimens. Again, due to the significant difference in masonry strength (9.5 vs 19.3 MPa), specimen TC constructed with C-shaped blocks had a higher ultimate capacity when compared to specimen TS constructed with stretcher blocks. Both specimens began to show noticeable cracking around 65% of the ultimate load. As shown in the failure modes of these specimens (see Figure 7), damages in the form of cracking and crushing were concentrated around midspan. The tensile crack extended through the midspan mortar joints and crushing occurred on the compression side. Both specimens showed the buckling of the longitudinal compressive reinforcement on the compression side of the specimen at failure.

Comparison of Specimens MC and TC

The behaviour of specimens MC and TC is compared in Figure 8 to demonstrate the effect of slenderness ratio. As shown in Figure 8(a) where the load vs. midspan lateral deformation curves are plotted, specimen

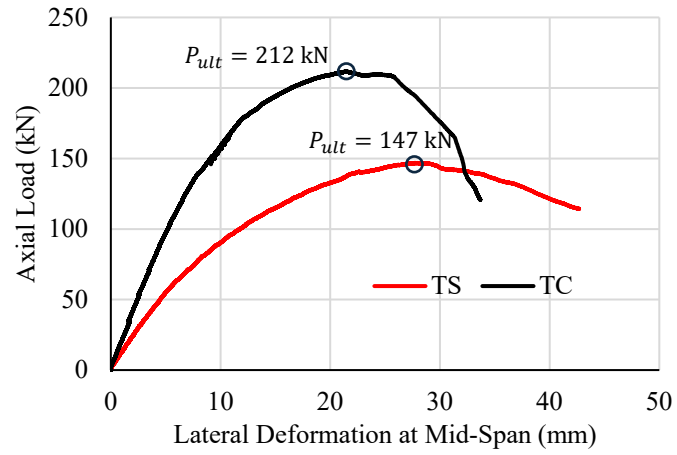
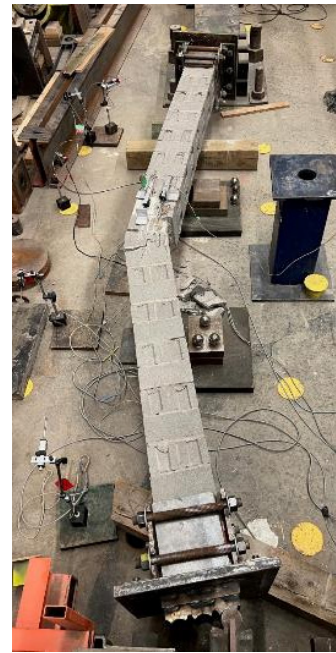


Figure 6: Load vs Midspan Lateral Deformation Curves for Specimens TC and TS



(a) Specimen TC

(b) Specimen TS

Figure 7: Failure Modes of Specimens TC and TS

TC with a higher slenderness failed at a lower load but experienced greater midspan deflection. The higher slenderness specimen also showed more pronounced nonlinearity in its load response throughout the loading history. The comparison of failure modes (see Figures 5 and 7) showed that specimen TC exhibited more extensive cracking and crushing at failure than specimen MC, which explains a more ductile failure as indicated in (a) Axial Load vs. Midspan Deformation (b) Moment vs Curvature

Figure 8(a) for specimen TC. **Error! Reference source not found.** compares the moment vs. curvature curves obtained at midspan for the two specimens. The moment was calculated as the product of the axial load and the combined initial eccentricity and the midspan deformation at failure. The curvature was determined using the strain readings at the midspan of the vertical reinforcement at failure as $(\epsilon_1 - \epsilon_2)/d$ where ϵ_1 and ϵ_2 are the average strains obtained at the compression and tension reinforcement and d is the distance between the two layers of reinforcement. The figure shows that the difference in midspan moment of the two specimens was not significant (18.4 vs. 18.9 kN.m). Although the axial capacity of the high slenderness specimen (TC) was markedly lower, the greater midspan deflection due to a higher slenderness, contributed to a much closer failure moment for these two specimens. The EI_{eff} values at failure was determined as the secant stiffness of the moment-curvature relationship and can be calculated as the slope of the line connecting the ultimate moment and the origin. It shows that an increase in slenderness from $kh/t = 12.6$ to 15.8 resulted in a 22% reduction in EI_{eff} . The high slenderness specimen attained a greater curvature at failure, and this, combined with a lower moment, resulted in a lower flexural rigidity.

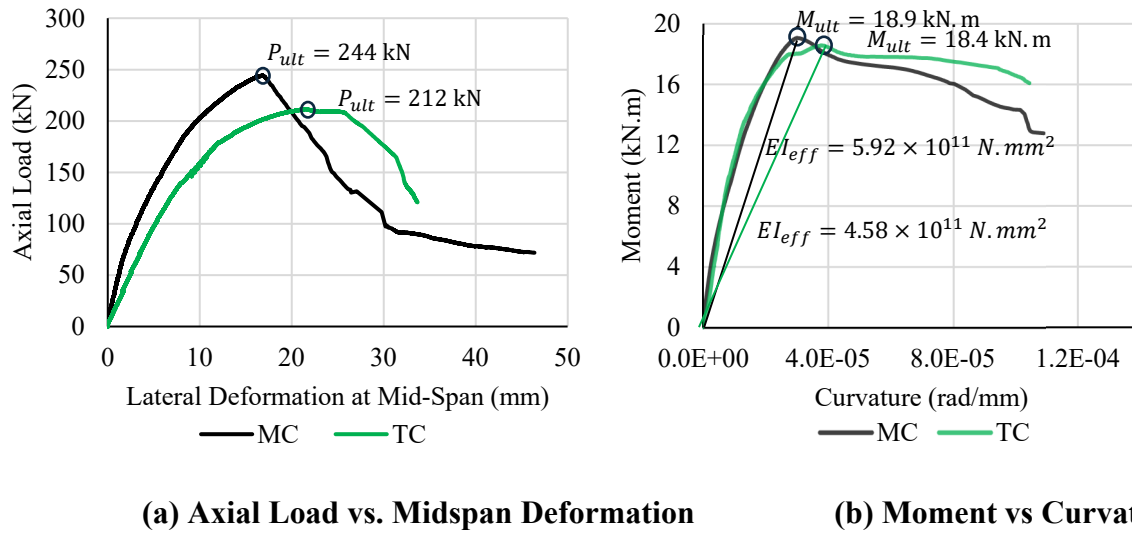


Figure 8: Behaviour Comparison of Specimens MC and TC

Comparison of Test Results with CSA S304 and TMS 402/602

For design of RM columns considering slenderness effect, both CSA S304 and TMS 402/602 adopts the moment magnifier method where the design moment is magnified to account for the slenderness effect through a one-step calculation using the Euler buckling concept. One key parameter in the Euler buckling load calculation is the so-called the effective flexural rigidity EI_{eff} , modified from the initial flexural rigidity to account for masonry cracking and reinforcement yielding at failure. However, in the calculation of EI_{eff} , CSA S304 and TMS 402/602 deviate significantly. In CSA S304, EI_{eff} is expressed as follows:

$$(1) \quad EI_{eff} = E_m \left[0.25I_o - (0.25I_o - I_{cr}) \left(\frac{e - e_k}{2e_k} \right) \right]$$

and the value of EI_{eff} shall not be greater than $0.25E_mI_o$, but need not be taken less than E_mI_{cr} . E_mI_o is the flexural rigidity of the uncracked cross-sectional area of the column, I_{cr} is the transformed moment of inertia of the cracked section, e and e_k are the equivalent applied eccentricity, and kern eccentricity, respectively. TMS 402/602 stipulates that I_{eff} shall be taken as $0.75I_n$ for $M_u < M_{cr}$ and shall be taken as I_{cr} for $M_u \geq M_{cr}$. In these relationships, M_{cr} is the column cracking moment capacity under bending, I_n is equivalent to I_o and I_{cr} is as defined above. It is noted that CSA S304-14 [1] stipulated that compressive load should be ignored in the calculation of I_{cr} . However, the new edition, S304-24, now requires that compressive load be considered. TMS 402/602 also requires considering the compressive load effect in calculation of I_{cr} .

Table shows the comparison of experimental results and values obtained from CSA S304-14 and TMS 402/602. It was found that under the new S304-24 provisions, the calculated I_{cr} was greater than $0.25I_o$ for all eccentrically loaded specimens. As a result, EI_{eff} would effectively be EI_{cr} , yielding the same value as TMS402/602. For comparison purpose, S304-14 provision for EI_{cr} calculation was instead used. In the table, P_{exp} and M_{exp} represent the experimentally obtained ultimate load, and the corresponding total moment measured at the midspan of specimens. The code ultimate load values, P_{CSA} and P_{TMS} , were determined by assuming M_{exp} values as the moment capacity of the column and then back calculating the ultimate axial load using the respective moment magnifier methods. Also shown for comparison are EI_{eff} values, determined experimentally and from the respective code equations and the magnification factor, δ , calculated as $1/(P-P_{cr})$. Since TMS 402/602 considers the axial load in the calculation of I_{cr} and thus I_{eff} and the ultimate load, P_{TMS} , were determined through an iterative process.

Table 3: Comparison of Test Results with Code Values

Spec. ID	Experimental Results				CSA S304-14			TMS 402/602		
	P_{exp} (kN)	M_{exp} (kN.m)	δ_{exp}	EI_{eff} (N.mm ² × 10 ¹¹)	P_{CSA} (kN)	EI_{eff} (N.mm ² × 10 ¹¹)	δ_{CSA}	P_{TMS} (kN)	EI_{eff} (N.mm ² × 10 ¹¹)	δ_{TMS}
SC	675	-		-	571	-		531	-	
SS	468	-		-	317	-		298	-	
MC	244	18.9	1.22	5.92	219	4.79	1.36	258	11.3	1.15
TC	212	18.4	1.37	4.58	181	4.54	1.60	225	9.37	1.29
TS	147	13.3	1.43	4.25	135	3.53	1.56	172	8.96	1.22

For the concentrically loaded specimens (SC and SS), the ultimate load values predicted by the two codes are similar, differing by only 7%, although both are lower than the experimental results. This indicates that for columns with low slenderness, both codes produce comparable designs. The slightly lower P_{TMS} values compared to P_{CSA} are due to the slenderness-dependent reduction factor applied to axial strength in TMS 402/602, even for columns with low slenderness. For eccentrically loaded specimens, the difference between CSA S304-14 and TMS 402/602 values is pronounced. While CSA S304 underestimates the ultimate load by an average 10.6%, TMS402/602 overestimates the ultimate load by an average 9.3%. The difference is evidently attributed to the significant difference in EI_{eff} values obtained from two codes, which in turn resulted in markedly different magnification factor, δ . Specifically, the TMS 402/602 method

yielded much greater EI_{eff} values - on average 2.3 times those of CSA S304-14 - which results in lower magnification factors, approximately 19% lower than those from CSA S304-14. It is noted that the CSA S304-14 EI_{eff} values were in a good agreement with the experimentally measured EI_{eff} values. Since the experimental EI_{eff} values were obtained at the column midspan, this suggests that the CSA S304-14 EI_{eff} equation is able to represent EI_{eff} at the location of maximum moment. On the other hand, while incorporating the axial load effect in calculation of EI_{eff} by TMS 402/602 is theoretically reasonable, the much higher EI_{eff} values as a result do not compare well with the experimental results. Given that S304-24 produces the same EI_{eff} values as TMS402/602, the comparison presented above raises questions on the effectiveness of modifying the I_{cr} calculation without updating the EI_{eff} equation.

CONCLUSIONS

Six masonry column specimens were tested to investigate the column behaviour and capacity as affected by cross-section configurations, slenderness, and eccentricity of axial load. The results were used to evaluate the efficacy of effective flexural rigidity equations specified in the Canadian and American masonry design standards. The failure modes of the specimens associated with their slenderness and loading conditions were presented and discussed. The comparison with the code EI_{eff} values showed that the S304-14 provision yielded better load predictions than TMS402/602 and S304-24 while the latter two would lead to unconservative load predictions. It is recommended that further experimental testing be conducted to validate these observations. Future tests should include a broader range of column slenderness ratios and include specimens subjected to reverse curvature bending.

ACKNOWLEDGEMENTS

The authors gratefully acknowledge the financial assistance provided by the NSERC Canada and Canadian Concrete Masonry Producers Association.

REFERENCES

- [1] Canadian Standards Association (CSA), 2014 or 2024. Design of masonry structures, CSA S304-14 or CSA S304-24. ed. Mississauga, ON, Canada.
- [2] Sturgeon, G., Longworth, J. & Warwaruk, J. (1971). "An Investigation of Reinforced Concrete Block Masonry Columns." Thesis, Department of Civil Engineering, University of Alberta, Alberta, Canada.
- [3] Edgell, G.J. and Templeton, W. (1985), "Reinforced Brickwork Columns," *Proc. 7th IBMAC*, Melbourne, Australia, pp 1065-1073.
- [4] Yokel, F. & Dijkers, R. D. (1971). "Strength of Load Bearing Masonry Walls." *Journal of the Structural Division*, 97(5), pp. 1593-1609.
- [5] Fattal, S. G. & Cattaneo, L. E. (1976). "Structural Performance of Masonry Walls Under Compression and Flexure." US Department of Commerce, National Bureau of Standards.
- [6] Hatzinikolas, M., Warwaruk, J. & Longworth, J. (1978). "Concrete Masonry Walls". Thesis. Department of Civil Engineering, University of Alberta, Alberta, Canada.
- [7] Ojinaga, J. & Turkstra, C. J. (1982). "Design of Reinforced Masonry Walls and Columns for Gravity Loads." *Canadian Journal of Civil Engineering*, 9(1), pp. 84-95.
- [8] TMS 402/602-16, 2016. Building Code Requirements and Specifications for Masonry Structures. The Masonry Society.
- [9] Liu, Y. & Hu, K. (2007). "Experimental Study of Reinforced Masonry Walls Subjected to Combined Axial Load and Out-of-Plane Bending". *Canadian Journal of Civil Engineering*, 34(11), pp. 1486-1494.
- [10] Isfeld, A., Muller, A., Hagel, M. & Shrive, N. (2019). "Analysis of Safety of Slender Concrete Masonry Walls in Relation to CSA S304-14." *Canadian Journal of Civil Engineering*, 46(5), pp. 423-438.

[11] CSA Group. (2014). CAN/CSA-A179-14: Mortar and Grout for Unit Masonry. Mississauga, ON: Canadian Standards Association.